High-resolution study of electron capture by 72- and 52-MeV ^{3}He projectiles from targets of high atomic number

I. Katayama* and H. Ikegami†
Research Center for Nuclear Physics, Osaka University, Mihogaoka, Ibaraki, Osaka 567, Japan

H. Ogawa
Department of Physics, Nara Woman's University, Nara 630, Japan

Y. Haruyama, M. Tozaki,‡ and A. Aoki§
Laboratory of Applied Physics, Kyoto Prefectural University, Sakyo-ku, Kyoto 606, Japan

F. Fukuzawa‖ and K. Yoshida
Department of Nuclear Engineering, Kyoto University, Sakyo-ku, Kyoto 606, Japan

I. Sugai
Institute for Nuclear Study, University of Tokyo, Tanashi, Tokyo 188, Japan
(Received 8 March 1994; revised manuscript received 1 September 1995)

An electron capture at the cyclotron energy has been explored by using a high-resolution magnetic spectrograph. The *K*-shell electron capture from heavy elements (V, Cr, Cu, Ge, Nb, Ag, and Sn) by $^3He^{2+}$ projectiles at 52 and 72 MeV was measured. The dependence of the cross sections on the atomic number of the target obtained at these two energies are compared with current electron-capture theories.

PACS number(s): 34.70.+e

I. INTRODUCTION

In electron capture a projectile ion picks up an electron from a target atom to a bound state of the projectile atom. Electron capture from the *K* shell of a heavy target atom by a light projectile ion at an intermediate energy has been studied both theoretically and experimentally [1]. Intermediate energy is defined as a region where the projectile velocity (v_p) is in between orbital velocities of v_i and v_f of the electron in the initial state of the target atom and in the final state of the projectile ion, respectively. The target atom is hereafter assumed to be far heavier than the projectile atom. Complications of electron capture at an intermediate energy arise from the fact that during a collision the distortion of the electron wave function in the Coulomb field due to the target atom is sufficiently large, and thus many states are required to perform channel-coupling calculations. Therefore, some approximations or truncations for the electron wave function during a collision are inevitably required.

The strong potential Born (SPB) theory, which inspired the present experiment, had been discussed enthusiastically [2]. In the SPB the stronger interaction of either the target or projectile nucleus with the electron to be captured is treated to the full order, and the weaker interaction is considered up to the first order. This theory had been tested by several experiments, such as a measurement of the Thomas peak for the $p+$He system [3] and the $p+$H system [4], the total cross sections for $^3He^{2+}$ on Ne and Ar targets [5], and shell identification of the final states in a heavy-ion projectile capturing an electron from a light target atom [6]. The SPB fairly well explains these data. Eichler and Dewangan, however, have found (though it had been already shown in Ref. [7]) that the initial-state component in the intermediate states in the SPB calculation gives a divergence term in the calculation [8]. They have, on the other hand, shown that by properly subtracting the distorting potential from the perturbation interaction (B1B) this problem may be solved. Since then, there has been quite a number of discussions concerning the proper treatment of the long-range Coulomb force in electron capture [9–12]. Despite the evolution of the electron-capture theories described above, there have not been many experiments concerning electron capture from the *K* shell of heavy target atoms for light projectiles at large projectile energies [13–15]. The heaviest target which has so far been reported is Ar, on which Horsdal-Pederson *et al*. measured the *K*-shell capture cross section of the target at a proton energy of 10 MeV [15]. They performed a coincidence measurement between the electron-capture product, i.e., neutral hydrogen H^0 and the deexcitation *K* x ray from the residual atom. Due to an increase in the incident energy and the target atomic number, this method is considered to be less effective due to the fact that the accidental coincidence because of the relative increase in *K* x ray fractions by ionization processes becomes serious. In this respect we have shown in previous reports that a high-resolution magnetic spectrograph can be successfully applied to separate the electron capture of a target *K* electron from the electron capture of an electron in higher shells [16,17]. It is to be noted that a magnetic spectrograph has also been shown to be effective for studying the

*Present address: INS, University of Tokyo.
†Present address: Dept. of Radiation Science, Uppsala University.
‡Present address: Radio Isotope Center, Kyoto University.
§Retired.
‖Present address: Fukuyama Technical College.

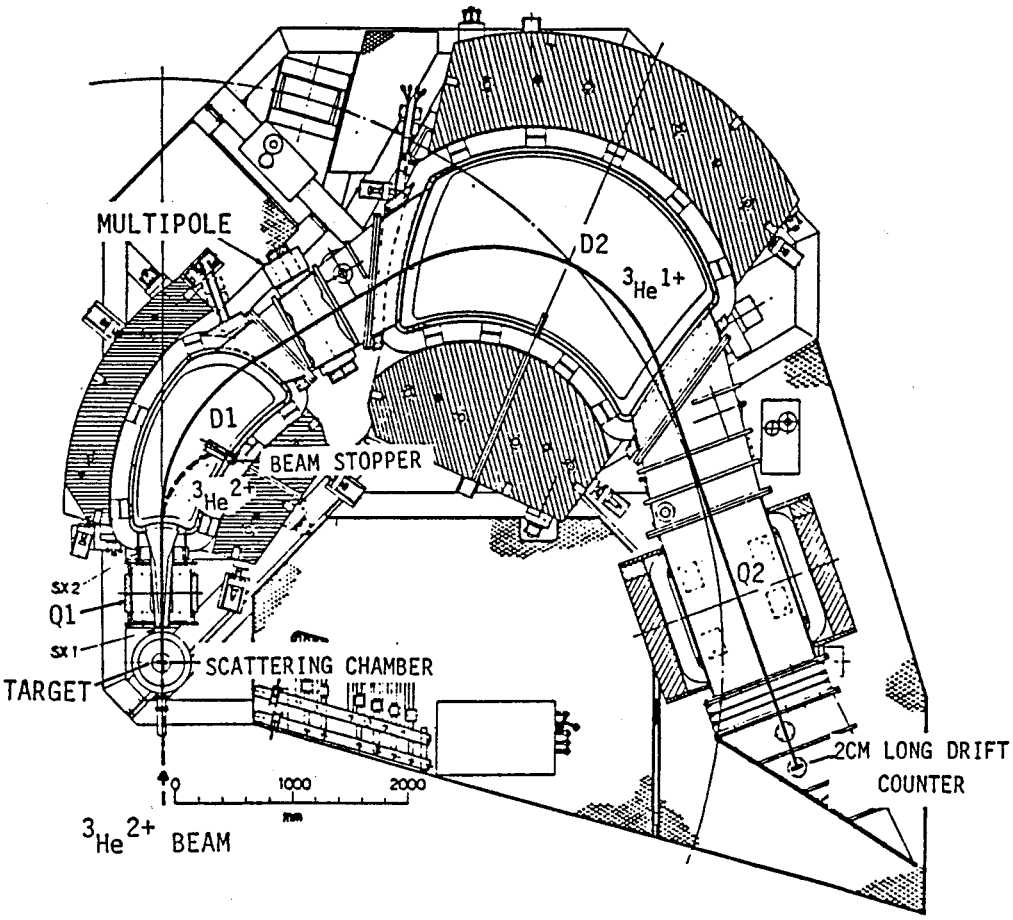

FIG. 1. Present experimental arrangement using the high-resolution magnetic spectrograph RAIDEN [19].

atomic collision process [18]. In the present paper we report on details concerning electron capture by 72- and 52-MeV $^3He^{2+}$ particles from the *K* shells of V, Cr, Cu, Ge, Nb, Ag, and Sn target atoms. For C and Al, although the total capture cross sections were measured, the *K*-shell contribution could not be separated. For a Au target, the upper limit of the capture cross section from the *K* shell is obtained. The contents of the present paper are as follows: Sec. II describes details concerning the experiment, and Sec. III deals with the experimental results. Section IV gives a comparison of the present results along with current theoretical predictions.

II. EXPERIMENTAL APPARATUS AND TARGET PREPARATION

A. Apparatus

Projectile $^3He^{2+}$ particles were accelerated and extracted from the AVF cyclotron at RCNP, Osaka University. The $^3He^{2+}$ particles were chosen because they provide the highest projectile velocity among available particles of which electron capture products still have a positive charge to allow for an energy analysis using a magnetic spectrograph. Two sets of a single quadrupole and a 90° dipole magnet in the beam-transport system form a beam monochrometer system having a length of 34 m. The aperture widths of the object, intermediate, and image slits were adjusted to be 0.5, 0.25, and 0.3 mm, respectively. The nominal momentum resolution obtainable by this analyzer system is nearly 5×10^{-5}; the best one obtained was 2×10^{-5}. Tuning of the cyclotron and beam analyzer to obtain a nominal resolution was relatively straightforward after some experience. It was, however, always painstaking to adjust the cyclotron so as to achieve a Gaussian-like beam profile in the momentum spectrum while also maintaining the resolution. A slight change in focusing the cyclotron beam on the first slit could cause a shift in the $^3He^{1+}$ peak position and/or a change in the line profile, especially at the low-energy tail of the main peak in the spectra (described later). It was therefore quite important that the magnet power supplies should have a very high stability for this experiment.

The present experimental arrangement using the magnetic spectrograph RAIDEN [19] is shown in Fig. 1. A highly momentum-resolved $^3He^{2+}$ beam was guided so as to hit the target in the scattering chamber of the spectrograph, which was positioned at zero degrees. The magnetic field was adjusted so as to measure the electron-capture product $^3He^{1+}$ at the focal plane counter; the $^3He^{2+}$ beams were stopped by an aluminum plate placed on the wall of the vacuum chamber of the first dipole magnet. The focal-plane counter was at first a 5-cm-long position-sensitive semiconductor detector (PSD), which was later replaced by a 2-cm-long single-wire drift gas counter followed by a 1-cm-thick plastic scintillator. The drift gas counter, which is a unit cell of a multiwire drift counter, has given a very stable position resolution of about 0.2 mm [17].

B. Preparation and thickness determination of the targets

Target foils having a size of 8×12 mm^2 were prepared by evaporating the target material on a thin (5 μg/cm^2) carbon

backing. The 12 targets were mountable in the scattering chamber at the same time. Because of the limited beam time, the thicknesses of only a half number of target foils were directly determined by the elastic scattering of 65-MeV protons. There has been a reliable and systematical analysis based on the optical-potential model for proton elastic scattering from various target nuclei at 65 MeV [20], which is the reason why this method was employed. The elastically scattered protons were measured at three angles around the first local maximum of the angular distribution of the differential cross sections. In the proton spectra the line from the C backing was well separated kinematically from target lines at these angles. The thickness of the target foils could be determined within an accuracy of 10% by this method. The thicknesses of the other remaining foils were determined from the relative yields of the elastic scattering of the 72-MeV ^{3}He beams. The elastically scattered $^3He^{2+}$ ions were measured at $\theta_{lab}=15°$, where the ^{3}He line from the target nucleus was also well separated from that of the C nucleus of the backing material. After the ^{3}He experiment, most of the targets used were again bombarded by a 2-MeV $^4He^{2+}$ beam from the van de Graaf accelerator at the department of Nuclear Engineering, Kyoto University, to perform a Rutherford backscattering (RBS) experiment. This allowed us to measure the thickness of the target as well as to examine the surface contamination of the targets. The details were reported in Ref. [21]. A further investigation of the contamination effect, including a list of all the targets, will be reported elsewhere [22].

III. MEASUREMENTS AND EXPERIMENTAL RESULTS

Three kinds of measurements (given below) were carried out in order to determine the cross sections of electron capture from the K shell of the target atoms.

A. Thickness dependence of the $^3He^{1+}$ total capture yields

The thickness dependence of the total $^3He^{1+}$ yields $[Y(t)]$ is given by

$$Y(t)=N_c\ \exp(-\sigma_1 t)+N_0(\sigma_t/\sigma_1)[1-\exp(-\sigma_1 t)], \qquad (1)$$

where σ_t is the total electron capture cross section for the reaction $^3He^{2+}+(\text{target})\rightarrow{}^3He^{1+}+(\text{target}')$, σ_1 the electron loss cross section for $^3He^{1+}+(\text{target})\rightarrow{}^3He^{2+}+e+(\text{target}')$, N_c the $^3He^{1+}$ yield from carbon backing, N_0 the beam intensity, and t the target thickness. Equation (1) is applicable when the carbon backing is facing the incoming beam; it was assumed that σ_1 is far larger than σ_t and that the neutral fraction of ^{3}He is negligibly small. The strength N_c was experimentally determined using a C foil of 5 μg/cm^2 in thickness as a target. The whole measurement was performed using only a scintillation counter at the focal plane of the spectrograph, because of the high counting rate of $^3He^{1+}$. The counting rate was, nonetheless, adjusted to be less than 10 000 cps by controlling the beam intensity. In order to measure the beam intensity, a sampling method was employed in this measurement. A thin polyethylene sheet, placed at about 10 m upstream of the target chamber, was intermittently inserted in the beam line, and elastically scattered ^{3}He particles from the sheet were detected by a NaI scintillation counter. The sheet was inserted for a few seconds every 10 s in order to eliminate any influence of the beam-intensity fluctuation on the $^3He^{1+}$ counts. Before and after each measurement, the ratio of the elastically scattered ^{3}He yields thus obtained to the integrated beam current measured with a Farady cup temporarily placed behind the target was determined. The obtained ratios agreed with each other within the statistical errors. In this way we could determine the integrated beam current within an accuracy of 3% in each measurement of the $^3He^{1+}$ yields. Figure 2 shows typical growth curves of the $^3He^{1+}$ yields at energies of 72, 62, and 52 MeV for Cu, Ge, Sn, and Au targets. The thickness dependence of the $^3He^{1+}$ yields was analyzed by a least-square fitting to Eq. (1), which enabled us to obtain σ_l and σ_t/σ_l. The RBS measurements described before showed that the Cu, Ge, and Ag targets were slightly oxidized on the surface. The influence of this effect on σ_t/σ_l was estimated using σ_t of oxygen, which was obtained by interpolating the σ_t of C and Al. The correction was less than 5%, at most. More details concerning this correction procedure will be reported elsewhere [22]. The final results of the thus-corrected σ_t/σ_l are summarized in Table I. The results of the cross sections σ_l were, however, independently measured by the attenuation method, which can give a more precise σ_l. The method and preliminary results are given in Ref. [21], and the final results are shown in Table I. We will not repeat every detail of the method, though the essential part of the method is described in the following section.

B. Attenuation measurement of $^3He^{1+}$

Intense $^3He^{1+}$ beams were first produced from the electron capture of $^3He^{2+}$ beams using a thin Au foil placed at the normal target position in the scattering chamber of the spectrograph. The $^3He^{1+}$ were then focused on a target material which was placed at the focal plane of the spectrograph. The charge state of ^{3}He particles coming out of the target material was analyzed by a small magnet located downstream of the focal plane. Both the $^3He^{1+}$ and $^3He^{2+}$ particles, separated by the magnet, were measured with a 4-cm-long position-sensitive gas proportional counter. This method gave an accurate attenuation of $^3He^{1+}$ intensity, and allowed us to obtain a more precise σ_l than that mentioned in the preceding section. By combining the thus-obtained σ_l with the previous σ_t/σ_l results we could determine the individual σ_l and σ_t, as mentioned in the preceding section. The results for the cross sections of the thus-obtained σ_t are listed in Table I. The errors for σ_l given in Table I come from the target thickness inaccuracy, which depends on each target and the least-squares fitting error. The errors for σ_t are determined based on the inaccuracies of σ_t/σ_l obtained from Eq. (1) and σ_l. The errors for σ_t/σ_l are from the correction inaccuracy of the surface-oxidization effect, which is at most 5%, and a charge-integration accuracy of around 3%. The errors of σ_t thus become about 13%, almost irrespective of the target species. An exception is the Ge target at 52 MeV, since the attenuation method could not be applied for this case. The σ_t data of Ge at 52 MeV in Table I was therefore obtained from the growth-curve method, as given by Eq. (1).

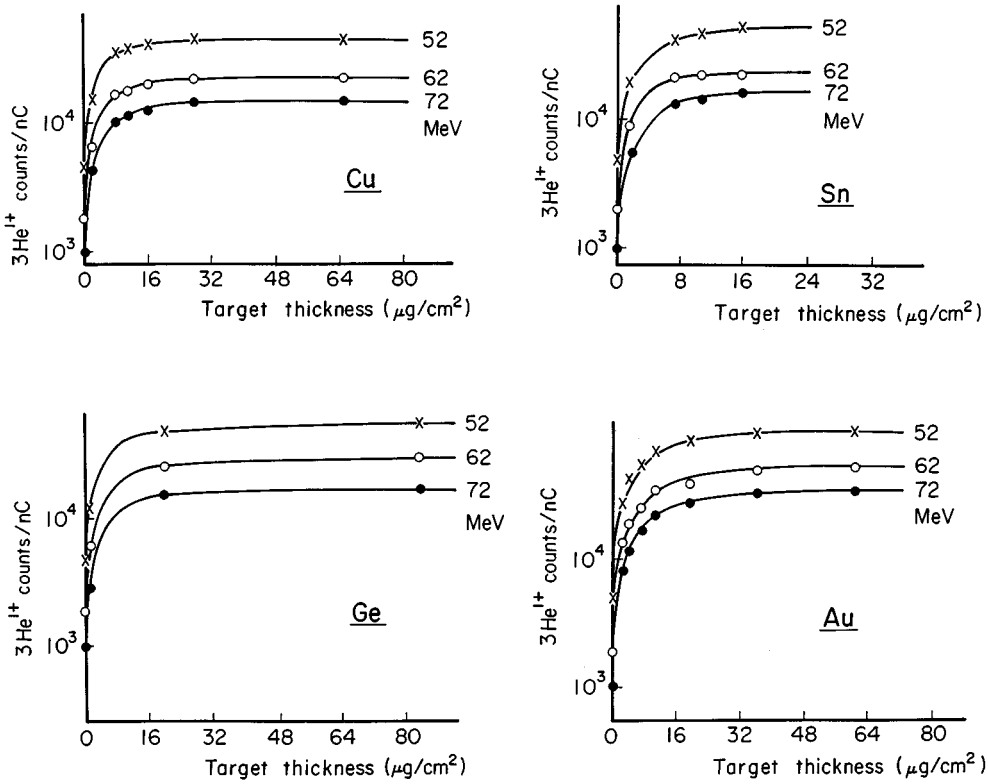

FIG. 2. Typical growth curves of the $^3He^{1+}$ yields at energies of 72, 62, and 52 MeV for Cu, Ge, Sn, and Au targets. The yields at zero thickness come from backing carbon. The results of a least-squares fitting to Eq. (1) are also indicated by solid lines.

C. High-resolution spectra of $^3He^{1+}$

The next measurement was for the separation of the K-shell contribution to the total capture cross section. The full width at half maximum (FWHM) of the peak from a C foil of 5 μg/cm^2 in thickness was 5.2 keV, which corresponds to 3.6×10^{-5} in momentum resolution. The energy spectrum of the direct beam was also measured, and gave the same momentum resolution as that of the $^3He^{1+}$ peak from the C mentioned above. This implies that there was no sizable line broadening due to electron capture in the carbon foil, and that the C line can thereby be used as a response function for the deconvolution of the $^3He^{1+}$ lines for the heavy target atom. The stability of the response function was checked before and after each measurement. The fraction of the momentum change in electron capture of $^3He^{2+}$ is given by

$$\Delta p/p=\tfrac{1}{2}\{\Delta_{\mathrm{BE}}/E(^3\mathrm{He})-m/M(^3\mathrm{He})\}, \qquad (2)$$

where Δ_{BE} is the binding-energy difference of the captured electron between the initial state of the target atom and the final state of the projectile atom, $E(^3\mathrm{He})$ and $M(^3\mathrm{He})$ are the kinetic energy and mass of the ^{3}He, respectively, and m is the electron mass. Since the binding energy of the final state in $^3He^{1+}$ is negligibly small compared to that of the initial state in the target atom in the present case, Δ_{BE} is almost equal to the binding energy of the initial state. From Eq. (2), the difference in the momentum changes between two lines in the $^3He^{1+}$ spectrum is given by

$$(\Delta p/p)_1-(\Delta p/p)_2=\tfrac{1}{2}(E_{B1}-E_{B2})/E(^3\mathrm{He}), \qquad (3)$$

where E_{B1} and E_{B2} correspond to the binding energies of each electron in initial states 1 and 2.

In Fig. 3, the $^3He^{1+}$ energy spectra obtained by the drift gas counter are shown for targets of C, Cu, Ge, Nb, Ag, Sn, and Au at a ^{3}He energy of 72 MeV. The thicknesses of all the targets for this measurement ranged from 5 to 10 μg/cm^2 on a 5μg/cm^2 carbon backing. Based on a momentum calibration of the spectra, we found that the small peaks seen at the right side of the main peaks in the spectra for Cu, Ge, and Nb targets have energy changes which correspond to the K-M-shell binding-energy difference from the main peaks for each element. It should be mentioned that energy-loss spectra of $^3He^{2+}$ for all of the targets were also measured. All the energy-loss spectra were found to be the same as the direct beam profile which was obtained without a target. This is because the energy loss and straggling is too small to be detected. The low-energy peaks for these three targets were therefore interpreted as being due to electron capture from the K shell of each target atom. The spectra for Cu and Ge targets were deconvoluted by a least-squares fitting analysis using the $^3He^{1+}$ spectrum of the C target as a response function. It is assumed that the smaller and larger peaks correspond to electron captures from the K shell, and the remaining higher shells plus backing carbon atoms, respectively. On the other hand, three lines were required for the Nb, Ag, and Sn targets from K, L, and other shells plus backing C and two lines for the Au target from L shell and other shells plus backing C. The analyzed results are shown in the figure by solid lines. The analysis gives us fractions of each target shell contribution to the total $^3He^{1+}$ yield, except for the K shells in the Ag and Sn cases. For the Ag and Sn targets, the deconvolution was made manually. One example of the result for the 72-MeV ^{3}He on the Sn target is shown in Fig. 4. The situation at 52 MeV and for the Ag target is quite similar to that shown in Fig. 4. In the spectra for Ge and Nb targets,

TABLE I. Present results of the total electron-capture cross sections (σ_t/atom), electron-loss cross sections (σ_l/atom), and electron capture from target K-shell cross sections (σ_K/atom) for 72- and 52-MeV $^3He^{2+}$ projectile. The theoretical predictions are also given for comparison.

		Experimental results			Theory (all in units of 10^{-7} πa_0^2/atom)				
Target	^{3}He[a] energy (MeV)	σ_t [b] (10^{-7} πa_0^2/atom)	σ_1 [c] (10^{-1} πa_0^2/atom)	σ_K [d] (10^{-7} πa_0^2/atom)	σ_K (MOBK)[e,f]	σ_K (eikonal)[g]	σ_K (SPB)[h,f]	σ_K (IA)[i,f]	σ_K (TSCM)[j,f]
C	72	0.031±0.003	0.26±0.026		0.214	0.067	0.077	0.0522	
	52	0.170±0.031	0.37±0.037		1.25	0.386	0.465	0.306	
Al	72	0.784±0.027	0.78±0.12		2.54	0.083	1.181	0.742	
	52	3.04±1.79	1.00±0.17		9.74	0.332	4.970	3.211	
V	72	2.28±0.29	2.91±0.37	0.99±0.15	3.03	1.033	1.886	1.463	
	52	8.02±1.06	3.95±0.51	2.86±0.43	6.44	0.230	4.599	4.025	
Cr	72	2.28±0.29	2.64±0.33	0.96±0.14	2.81	0.983	1.802	1.439	
	52	9.05±0.99	3.67±0.48	2.36±0.35	5.67	0.203	4.183	3.800	
Cu	72	2.60±0.29	2.20±0.23	0.475±0.07	1.69	0.597	1.251	1.165	1.25
	52	14.5±1.8	4.01±0.45	1.53±0.23	2.68	0.999	2.313	2.532	1.52
Ge	72	2.75±0.30	2.24±0.23	0.46±0.07	1.16	0.418	0.929	0.952	0.74
	52	14.2±3.2	1.77±0.45	0.91±0.25	1.61	0.621	1.516	1.856	0.72
Nb	72	4.64±0.57	3.32±0.43	0.085±0.012	0.301	0.124	0.307	0.418	
	52	17.0±2.0	4.07±0.49	0.092±0.014	0.290	0.140	0.362	0.613	
Ag	72	4.33±0.51	2.55±0.28	0.021±0.010	0.110	0.053	0.133	0.217	0.022
	52				0.086	0.0525	0.130	0.270	0.007
Sn	72	4.66±0.59	4.36±0.54	0.011±0.005	0.065	0.035	0.086	0.153	
	52	17.0±2.0	5.44±0.61	0.010±0.002	0.047	0.0327	0.077	0.177	
Au	72	15.7±2.2	6.73±0.91	<0.001	0.0004	0.009	0.0010	0.004	
	52	57.2±7.4	7.72±0.92	<0.001	0.0002	0.0006	0.0005	0.003	

[a]Growth curve data were also measured at 62 MeV (see Fig. 2). The results are not included in this table.
[b]Oxidization effect is corrected, which is less than 5% at most.
[c]Our data.
[d]Obtained from Eq. (4).
[e]MOBK calculation for K capture (Ref. [27]).
[f]A factor 2.4 is multiplied to $K\rightarrow K$ cross sections. The factor 2 contained is from two K electrons in target atoms and the other 1.2 is from the sum of $1/n^3$ ($n\geq 2$), where n is the principal quantum number of projectile states.
[g]Eikonal approximation for K capture (Ref. [29], sum of partial cross sections to different projectile states).
[h]SPB calculation (Ref. [31]).
[i]Impulse approximation (Ref. [32]).
[j]TSCM (see text) calculation (Ref. [28]).

due to the existence of a small second component in the incident-beam energy distribution, which is clear based on the C spectrum, it has an effect to somewhat bury the valley between the peaks of the higher shells and the K shell. The measurements of $^3He^{1+}$ spectra were carried out many times spanning almost four years. For each measurement, the response line was always measured, since it is not only the key data used to analyze the spectra, but also to monitor the beam stability. The spectra shown in Fig. 4 represent only one of the examples. The final results are obtained after summarizing all of the data. It is worth mentioning that the momentum change of ^{3}He due to the second term of Eq. (2) was recently measured at RCNP. The details concerning the measurement are given in Ref. [23].

The K-shell capture cross sections were obtained from the following relation:

$$\sigma_K=\sigma_t\,\frac{K}{K+L+M+\cdots+C}\,\frac{K+L+M+\cdots+C}{K+L+M+\cdots}, \quad (4)$$

where $K,L,M,\ldots,C$ denote the $^3He^{1+}$ components stemming from each target shell $(K,L,M,\ldots)$ and from the backing carbon of each target. The σ_t is that obtained from Eq. (1). The second factor is obtained from a deconvolution of the $^3He^{1+}$ spectrum. The last factor is deduced from Eq. (1) as $Y(t_l)/[Y(t_1)-N_c\exp(-\sigma_l t_l)]$, which is calculable for a specific target thickness (t_l) of the target used to measure the $^3He^{1+}$ energy-loss spectrum. The thus-obtained K-shell electron capture are also summarized in Table I. By applying almost the same procedure as that for the L-shell lines, we could also deduce the L-shell electron-capture cross sections. A preliminary result for L capture has already been reported in Ref. [24].

IV. DISCUSSION

Before comparing our data with theoretical predictions, the effect of a two-step process on the data must be clarified. The two-step process here means the ionization or excitation

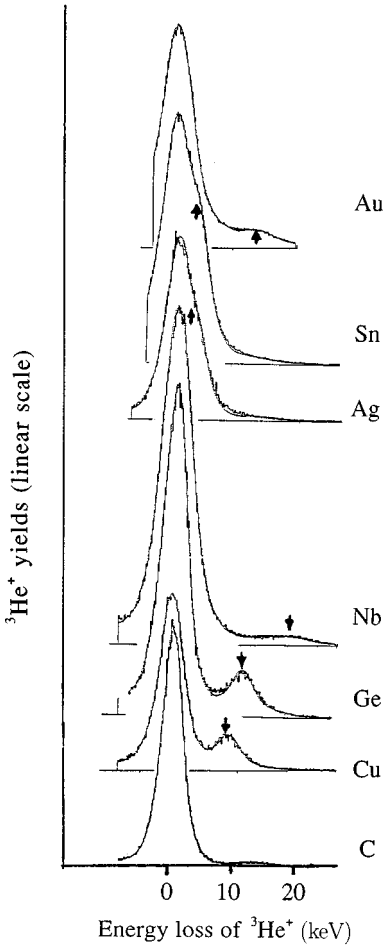

FIG. 3. Typical $^3He^{1+}$ energy spectra measured under the same condition for C, Cu, Ge, Nb, Ag, Sn, and Au targets at an incident energy of 72 MeV. For V and Cr targets, it was measured in a different run. The arrow pointing downwards indicates the *K*-shell position of the corresponding target atom, and the upward indicates the *L*-shell position. The solid lines are the results of peak fitting using the C-line shape (for details, see the text). A small bump observed in case (c) is due to the beam structure.

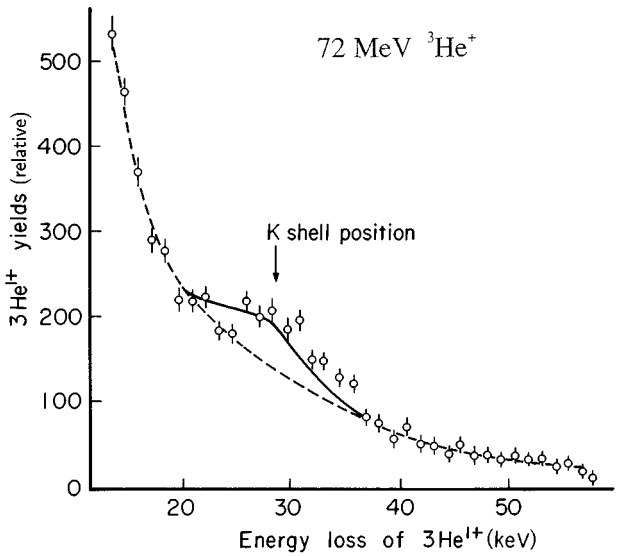

FIG. 4. Deconvolution of the *K*-shell line in a Sn target.

of an inner-shell electron of an atom to the outer shell followed by the capture of one of the outer-shell electrons of the target atoms by a projectile. This process cannot be excluded in our experimental method, since it also gives the same momentum change as that of the $^3He^{1+}$, which captures the *K*-shell electron. There are two possibilities of this process, i.e., that due to a single collision or to a double collision. We will show in the following that both cases can be safely neglected in the present experiment. We first consider a single-collision case [25]. The cross section of the process σ_{scoll} is given approximately as the product of $\sigma_{\text{ion}}(\sigma_{HC}/\pi a_0^2)$, where σ_{ion} is the cross section to ionize or excite a *K*-shell electron to a higher empty shell of the atom, σ_{HC} the capture cross section of any electron in higher shells by the projectile ion, and πa_0^2 the geometrical cross section in the upper limit for electron capture of the higher shell. The $(\sigma_{HC}/\pi a_0^2)$ is thus the probability for electron capture from the higher shell. The σ_{ion}'s are obtained from Ref. [26]. The factors $\sigma_{\text{ion}}/(\pi a_0^2)$ for collisions of present interest were found to be about 10^{-5}. A number, which is the product of this factor and σ_{HC}, can give a rough estimate of the cross section (σ_{scoll}). The ratio $\sigma_{\text{scoll}}/\sigma_t$ gives the fraction of the two-step process contribution in the total capture cross section. The ratio is given as $[\sigma_{\text{ion}}/(\pi a_0^2)]$ (σ_{HC}/σ_t) using the above result. The quantity σ_{HC} is almost of the same order as the σ_t. The ratio thus becomes nearly 10^{-5}, which is quite small compared with σ_K/σ_t of the experimental results given in Table I. This two-step process can thus be safely neglected. The second case is due to a double collision, i.e., subsequent collisions in a target. The fraction of this contribution is approximately given as

$$Y_{\text{dcoll}}/Y_t = 0.5(\sigma_{HC}/\sigma_t)\sigma_{\text{ion}}t, \tag{5}$$

where Y_{dcoll} is the *K*-shell peak intensity due to double collisions, Y_t the total capture yield, and t the target thickness in atoms/cm^2. The right-hand part of Eq. (5) gives nearly 10^{-5}, irrespective of the kind of target, which is again quite small compared to the σ_K/σ_t ratios given from Table I. It should be also noted that the result of Eq. (5) shows linear dependence on the target thickness. Related to this problem, we have also made a measurement similar to the one described in Fig. 3 for targets with different thicknesses. For example, measurements for three Nb targets, (1.4, 4.2, and 8.8 μg/cm^2) at 72 MeV gave the $(\sigma_K/\sigma_t)^{-1}$ ratios which agree within the error bars (22 ± 4, 16 ± 2, and 17 ± 2, respectively). Other data of the σ_K/σ_t ratios also did not show any linear dependence on the target thickness. Based on these discussions, we have concluded that the experimental data given by Eq. (4) can give the electron-capture cross section for the *K* shell of targets.

In Fig. 5(a) [5(b)], the present results for the σ_K of the 72-MeV (52-MeV) $^3He^{2+}$ as a function of the target atomic number (Z_t) are shown together with the theoretical predictions. The numerical results of theoretical predictions are

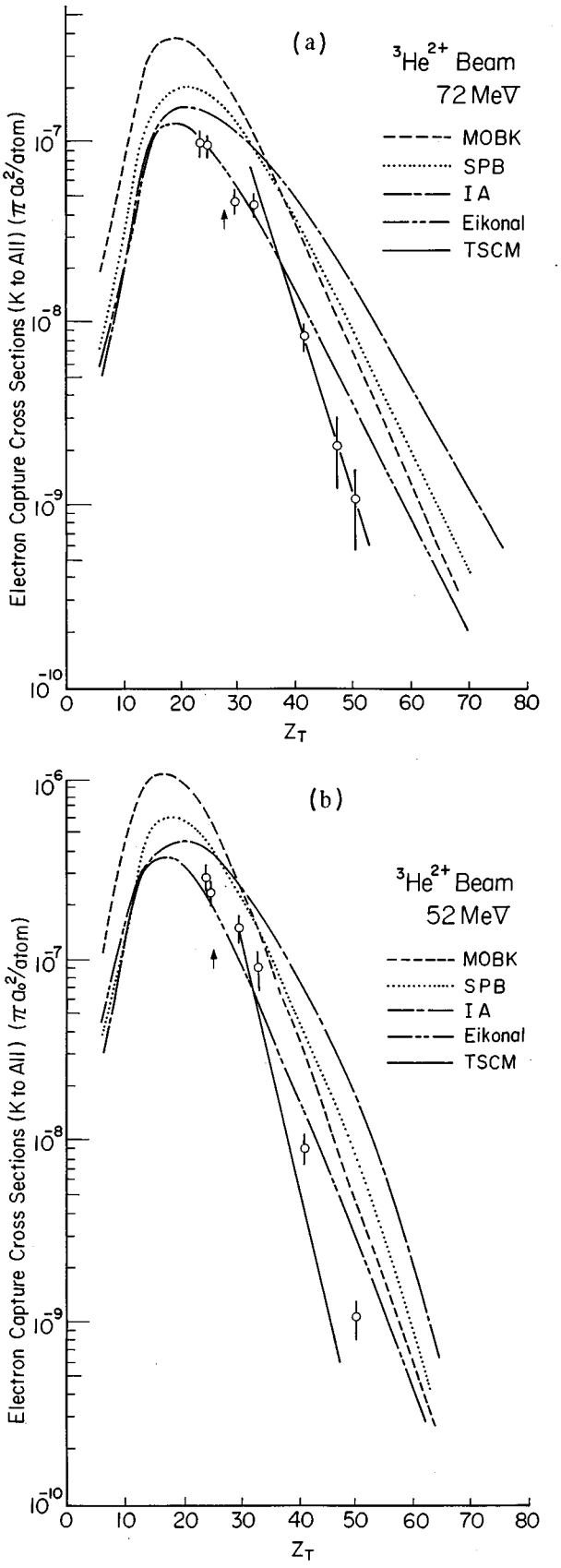

FIG. 5. Z_t dependence of the target K-shell electron-capture cross sections of our experimental results together with theoretical calculations (for details, see text) (a) for 72-MeV $^3He^{2+}$, (b) for 52-MeV $^3He^{2+}$.

also tabulated in Table I. The arrow in the figure gives the atomic number at which the 72-MeV (52-MeV) ^{3}He projectile velocity is equal to the velocity of the classical orbital motion of a K electron in the target atom [$V_1=31\ v_0$ ($26v_0$) for 72 MeV (52 MeV), where v_0 is the Bohr velocity]. The MOBK is a modified OBK theory by Kuang, where a correlation effect between the active and passive electrons has been considered in some approximation [27]. A two-state coupling model (TSCM) has been proposed by Lin [28]; the calculation is indebted to Toshima. According to Toshima, along with an increase of Z_t in heavy targets, the perturbation method becomes less effective, although the TSCM still maintains its effectiveness. This is because in heavy targets the K-shell orbit is quite well separated from the other orbits, and thus TSCM is justified. TSCM well explains our data for heavy targets. On the other hand, the eikonal theory [29] explains the velocity dependence of the cross section in light elements. It is to be noted, however, that, according to Eichler, the eikonal theory has a sound region where the projectile velocity is at least twice larger than the K-shell orbital velocity [30]. Thus, the agreement of our data with the eikonal calculation for targets heavier than Cu is kind of marginal. Dewangen and Eichler have recently reviewed the status of electron-capture theory [12]. They have emphasized the importance of the Coulomb boundary condition. The residual interaction $Z_t(Z_p-1)/R$ was discussed by them, where Z_p is the atomic number of the projectile and R is the internuclear distance between the target and the projectile. This interaction becomes zero in the case of the $p+\mathrm{Ar}\rightarrow\mathrm{H}^0+\mathrm{Ar}^{1+}$ experiment [15], whereas it can not be neglected in the present case. In this regard, it is quite interesting to see how the Coulomb boundary-corrected first-order Born approximation (B1B) and the second-order approximation (B2B) can explain our result.

The numerical results of the SPB approximation by McGuire *et al.* [31] and the impulse approximation (IA) by Briggs [32] are also given in Figs. 5(a) and 5(b) and Table I. In the SPB approximation as well as the IA, V_1/Z_t is an important quantity for discussing the effectiveness of perturbation theories. The previous $p+\mathrm{Ar}\rightarrow\mathrm{H}^0+\mathrm{Ar}^{1+}$ experiment corresponds to $V_1/Z_t=1.1$. Also, in the present 72-MeV and 52-MeV $^3\mathrm{He}^{2+}$ electron-capture experiments, V_1/Z_t ranges from 0.5 to 1.3. Although the present data are in the V_1/Z_t region where the SPB approximation is effective, the calculations cannot reproduce the data. In this connection, the SPB calculations developed in the 1980s have lost their sound basis, as mentioned before. Nevertheless, they give finite numerical values due to the peaking approximation. The SPB calculations quoted in our paper are those obtained with the peaking approximation. Therefore it is desired to compare the present data with the theoretical values based on the newly revised SPB [11] in order to discuss the validity of the SPB approximation.

As a conclusion, the employment of a high-resolution magnetic spectrograph for electron capture at the cyclotron energy has made it possible to observe the target-shell effect. The present experiment for the electron capture of $^3\mathrm{He}^{2+}$ at 72 and 52 MeV from K shells of the target atoms hopefully

provides the basis for a stringent test of electron-capture theories.

ACKNOWLEDGMENTS

We acknowledge S. Morinobu, M. Fujiwara, and T. Noro for their contribution during the early stage of the experiment. We also acknowledge J. H. McGuire for sending us computer programs to calculate the SPB and IA and J. Eichler for eikonal results. Thanks are also due to N. Toshima for his calculation of the TSCM result, K. Ishii for providing information concerning the two-step process, and H. Schuessler for reading the manuscript.

[1] Experimental works are, for example, those of Refs. [3,13–17] and also the contributions by S. Andriamonje *et al.*, *International Conference on the Physics of Electron-Atom Collisions*, edited by S. Datz (North-Holland, Amsterdam, 1981), p. 657; on the other hand the theoretical works are those of Refs. [2,7–12,27–32].

[2] J. Macek and K. Taulbjerg, Phys. Rev. Lett. **46**, 170 (1981); J. Macek and S. Alston, Phys. Rev. A **26**, 815 (1982).

[3] E. Horsdal-Pedersen, C. L. Cocke, and M. Stockli, Phys. Rev. Lett. **50**, 1919 (1983).

[4] H. Vogt, R. Schuch, E. Justiniano, M. Schultz, and W. Schwab, Phys. Rev. Lett. **57**, 2256 (1986).

[5] I. Katayama, G. P. A. Berg, W. Hürlimann, S. A. Martin, J. Meissburger, W. Oelert, M. Rogge, J. G. M. Römer, L. Tain, L. Zemlo, and G. Gaul, J. Phys. B **17**, L23 (1984).

[6] A. Jolly, K. Wohrer, A. Chetioui, J. P. Rozet, C. Stephan, and L. J. Dube, J. Phys. B **17**, 235 (1984).

[7] Dz. Belkic, R. Gayet, and A. Salin, Phys. Rep. **56**, 279 (1979).

[8] D. P. Dewangan and J. Eichler, J. Phys. B **18**, L65 (1985).

[9] J. H. Macek, J. Phys. B **24**, 5121 (1991).

[10] A. Salin, J. Phys. B **25**, L137 (1992).

[11] H. Marxer and J. S. Briggs, J. Phys. B **25**, 3823 (1992).

[12] D. P. Dewangan and J. Eichler, Phys. Rep. **247**, 59 (1994).

[13] C. L. Cocke, R. K. Gardner, B. Curnutte, T. Bratton, and T. K. Saylor, Phys. Rev. A **16**, 2248 (1977).

[14] W. Schwab, G. B. Baptista, E. Justiniano, R. Schuch, H. Vogt, and E. W. Weber, J. Phys. B **20**, 2825 (1987).

[15] E. Horsdal-Pedersen, C. L. Cocke, J. L. Rasmussen, S. L. Varghese, and W. Waggoner, J. Phys. B **16**, 1799 (1983).

[16] I. Katayama, M. Fujiwara, S. Morinobu, T. Noro, H. Ikegami, F. Fukuzawa, and I. Sugai, in *Proceedings of the 2nd Asia-Pacific Physics Conference, Bangalore, 1986*, edited by S. Chandrasekhar (World Scientific, Singapore, 1986), p. 662.

[17] H. Ogawa, I. Katayama, Y. Haruyama, T. Noro, H. Ikegemi, F. Fukuzawa, K. Yoshida, A. Aoki, and I. Sugai, Nucl. Instrum. Methods A **262**, 23 (1987).

[18] R. Schuch, H. Schöne, P. D. Miller, H. F. Krause, P. F. Dittner, S. Datz, and R. E. Olson, Phys. Rev. Lett. **60**, 925 (1988).

[19] H. Ikegami, S. Morinobu, I. Katayama, M. Fujiwara, and S. Yamabe, Nucl. Instrum. Methods **175**, 335 (1980).

[20] H. Sakaguchi, M. Nakamura, K. Hatanaka, A. Goto, T. Noro, F. Ohtani, H. Sakamoto, H. Ogawa, and S. Kobayashi, Phys. Rev. C **26**, 944 (1982).

[21] Y. Haruyama, I. Katayama, H. Ogawa, T. Noro, H. Ikegami, F. Fukuzawa, K. Yoshida, A. Aoki, and I. Sugai, Nucl. Instrum. Methods B **33**, 220 (1988).

[22] Y. Haruyama, I. Katayama, H. Ogawa, M. Ikegami, M. Tozaki, A. Aoki, F. Fukuzawa, K. Yoshida, and I. Sugai (unpublished).

[23] H. Ogawa, I. Katayama, H. Ikegami, Y. Haruyama, A. Aoki, M. Tosaki, F. Fukuzawa, K. Yoshida, I. Sugai, and T. Kaneko, Phys. Rev. B **43**, 11 370 (1991).

[24] H. Ogawa, I. Katayama, T. Noro, H. Ikegami, Y. Haruyama, A. Aoki, F. Fukuzawa, K. Yoshida, and I. Sugai, in *Proceedings of the 3rd Workshop on High Energy Ion-Atom Collision Processes*, Lecture Notes in Physics Vol. 294, edited by D. Berenyi and G. Hock (Springer-Verlag, Berlin, 1988), p. 145.

[25] D. L. Matthews, *Methods of Experimental Physics* (Academic, New York, 1980), Vol. 17, p. 487.

[26] D. D. Cohen and M. Harrigan, At. Data Nucl. Data Tables **33**, 255 (1985).

[27] Y. R. Kuang, Phys. Rev. A **44**, 1613 (1991).

[28] C. D. Lin, S. C. Soong, and L. N. Tunnell, Phys. Rev. A **17**, 1646 (1978).

[29] J. Eichler, Phys. Rev. A **23**, 498 (1981).

[30] J. Eichler (private communication).

[31] J. H. McGuire, R. E. Kletke, and N. C. Sil, Phys. Rev. A **32**, 815 (1985).

[32] J. S. Briggs, J. Phys. B **10**, 3075 (1977).